Charge Transfer

Observation and Dynamics of "Charge-Transfer Isomers"**

Tasuku Ito, Naoyuki Imai, Tadashi Yamaguchi, Tomohiko Hamaguchi, Casey H. Londergan, and Clifford P. Kubiak**

We previously reported the measurement of rates of electron transfer (ET) by the coalescence of vibrational absorption bands in infrared (IR) spectra.[1,2] To observe the coalescence of vibrational bands in IR spectra, rates of chemical exchange

[*] Prof. T. Ito, N. Imai, Dr. T. Yamaguchi
Department of Chemistry, Graduate School of Science
Tohoku University. Sendai 980–8578(Japan)
Fax: (+81) 22-217-6548
E-mail: ito@agnus.chem.tohoku.ac.jp
Dr. C. H. Londergan, Prof. C. P. Kubiak
Department of Chemistry and Biochemistry
University of California
San Diego, La Jolla, CA 92093–0358 (USA)
Fax: (+1) 858-822-2665
E-mail: ckubiak@ucsd.edu
T. Hamaguchi
PRESTO, Japan Science and Technology Corporation
Sendai 980-8578 (Japan)

[**] This work was supported by Grant-in-Aid for Scientific Research (Priority Area "Metal Assembled Complexes" No. 10149102) from the Ministry of Education, Culture, Sports, Science, and Technology, and The U.S.—Japan Cooperative Science Program from JSPS and NSF. CPK and CHL gratefully acknowledge support from NSF (CHE-0079182) and an International Travel Award (INT-0087420) to support collaborative studies with the Ito research group.

  DOI: 10.1002/ange.200353221

must be very fast, about 10^{11}–10^{12} s^{-1}.[1–3] The dynamic exchange observed in singly reduced symmetric intervalence charge-transfer complexes, $[A–A]^-$, occurs between the two equivalent charge distributions related by ET: $[A^––A]\rightleftarrows[A–A^–]$. Simulation of the extent of vibrational band coalescence in the IR spectrum can then be used to estimate the ET rate constants.[1,2] We now report the application of this method to study asymmetric charge-transfer complexes of the type $[A–B]^-$. We report several unprecedented findings, including the spectroscopic observation of both of the two possible charge-transfer isomers, for example, $[A^––B]$ and $[A–B^–]$, and dynamic exchange between them on the picosecond timescale.

In contrast to a symmetric charge-transfer complex $[A–A]^-$, intramolecular electron transfer in an asymmetric system $[A–B]^-$ is somewhat complicated. The question of whether an electron transfer will proceed within an asymmetric mixed valence state depends on two factors: (1) ΔG, the "driving force" or difference in free energy to attain $[A–B^–]$ starting from $[A^––B]$; (2) H_{AB}, the electronic coupling matrix element that quantum mechanically mixes the potential energy surfaces for $[A^––B]$ and $[A–B^–]$, stabilizes the resulting symmetric combination (lower surface), and destabilizes the antisymmetric combination (upper surface). This produces an energy separation of $2H_{AB}$ between the lower and upper surfaces at the crossing point (Figure 1). One

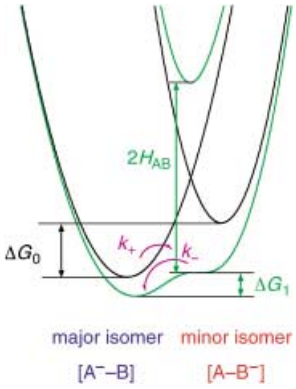

Figure 1. Marcus–Hush semiclassical model to describe ET in asymmetric charge transfer complexes, $[A–B]^-$.

complication of asymmetric mixed valency is that increased contributions of H_{AB} or ΔG work in opposite directions. Increases in H_{AB} tend to delocalize the electronic charge between A and B, whereas increases in ΔG tend to localize (trap) the charge. A more serious complication is that ΔG depends on H_{AB}. Note that electronic coupling (H_{AB}) has the effect of decreasing the free energy change for electron transfer from a value ΔG_0 in the diabatic case ($H_{AB}=0$) to a value of ΔG_1 in the adiabatic case. One special case that has escaped both experimental observation and theoretical discussion in the literature is that in which H_{AB} and ΔG are of appropriate magnitudes to permit the coexistence of similar populations of the two possible charge-transfer isomers: $[A^––B]$ and $[A–B^–]$. These could then exist as a major and a minor isomer, which exchange identity by intramolecular electron transfer. In particular, ET in the major isomer results in the formation of the minor isomer, and vice versa. In this letter, we present experimental evidence for the existence of such charge-transfer isomers. We describe how vibrational-band intensities and lineshapes in the IR are used to determine directly the difference in Gibbs free-energy, ΔG_1, and electron-transfer kinetics for strongly coupled asymmetric charge-transfer complexes.

The asymmetrical complexes $[Ru_3O(OAc)_6(L)(CO)(\mu\text{-}pz)Ru_3O(OAc)_6(L')(CO)]$ (pz = pyrazine, L = 4-dimethylaminopyridine (dmap), L′ = pyridine (py), **1**; L = py, L′ = 4-cyanopyridine (cpy), **2**; L = dmap, L′ = cpy, **3**) were prepared by modification of the procedures used to synthesize the symmetrical complexes. Each complex (**1**–**3**) displays two single-electron reduction waves in its cyclic voltammogram that correspond formally to $Ru_3^{III,III,II}$-pz-$Ru_3^{III,III,II}$/$Ru_3^{III,III,II}$-pz-$Ru_3^{III,II,II}$ (0/−1 overall charge) and then $Ru_3^{III,III,II}$-pz-$Ru_{33}^{III,II,II}$/$Ru_3^{III,II,II}$-pz-$Ru_3^{III,II,II}$ (−1/−2 overall charge; see Figure 2). This is completely analogous to the situation found in the symmetric complexes.[1,2] However, in contrast to the symmetric complexes, the magnitude of splitting between the two single-electron reduction waves, (0/−1) and (−1/−2), not only reflects the electronic interaction between the two Ru_3 clusters but also the difference in their intrinsic reduction potentials because of the different ligands present. The total splittings for the single-electron reductions of **1**–**3** are 410 mV

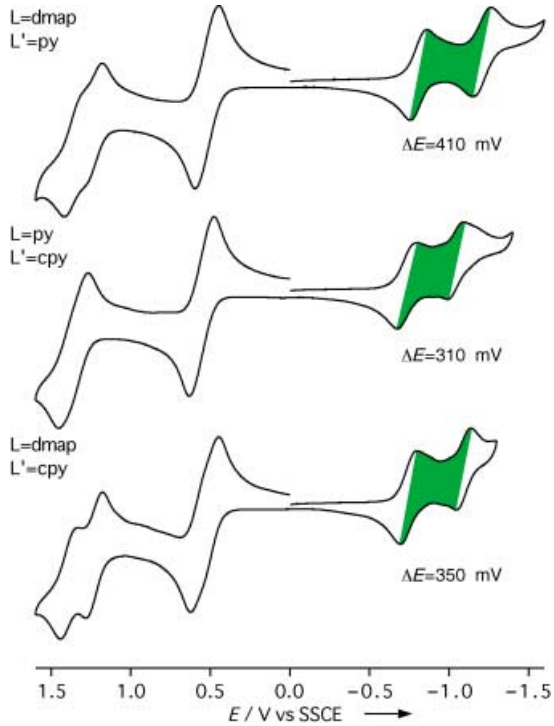

Figure 2. Cyclic voltammograms of the asymmetrically ligand substituted complexes: L = dmap, L′ = py (**1**); L = py, L′ = cpy (**2**); L = dmap, L′ = cpy (**3**). The two sequential single-electron reduction waves correspond to the (0/−1) and (−1/−2) redox processes. The measured splittings, ΔE, between the (0/−1) and (−1/−2) reduction waves reflect both the differences in intrinsic reduction potentials that depend on the ligands present and the degree of intercluster electronic coupling. SSCE = sodium-saturated calomel electrode.

(**1**), 310 mV (**2**), and 350 mV (**3**). These compare with differences in intrinsic reduction potentials of the clusters, which depend only on the ligand set present,[4] 100 mV (**1**), 130 mV (**2**), and 230 mV (**3**). Thus, the differences in electrochemical splittings observed are significantly larger than the differences in intrinsic reduction potentials, which suggests that large intercluster electronic interactions exist in the mixed valence (−1) states of **1**–**3** (large H_{AB}). The differences in intrinsic reduction potentials also provide a reasonable estimate of ΔG_0, the Gibbs free energy for transferring an electron from a Ru_3 cluster with one type of ligand substitution to another in the absence of any perturbation from electronic coupling, H_{AB}.

The mixed valence (−1) states of **1**–**3** exhibit intense intervalence transfer (IT) absorptions in their electronic spectra.[5] This provides additional evidence of the high degree of electronic coupling that is present in the mixed valence states. Because these IT electronic-absorption bands are relatively broad and overlapped with other electronic transitions, it is not possible to resolve charge-transfer isomers. However, resolution can be achieved by vibrational spectroscopy. The vibrational spectra of the mixed-valence (−1) state were obtained using a custom low-temperature reflectance IR spectroelectrochemical (SE) cell under potentiostatic control.[6] The carbonyl stretching (ν(CO)) bands contain the most pertinent information. The ν(CO) spectra of the singly reduced states of **1**–**3** exhibit two broad and extensively overlapped bands, whereas the neutral (0) and doubly reduced (−2) states show single ν(CO) bands at higher and lower energy, respectively. The ν(CO) bands of **1** in the neutral (0), mixed valence (−1), and doubly reduced (−2) states are presented in Figure 3. In the case in which major and minor charge-transfer isomers exist in the spectrum of the mixed valence (−1) state, there will be four components to the overall ν(CO) spectral lineshape (Figure 4): (1) An intense high-frequency component from the unreduced cluster containing ligand L: major (L). (2) An intense low-frequency component from the reduced cluster containing ligand L′: major (L′). (3) A weak high-frequency component from the unreduced cluster containing ligand L′: minor (L′). (4) A weak low-frequency component from the reduced cluster containing ligand L: minor (L). Electron transfer within the major and minor isomers leads to two simultaneous two site chemical exchanges: major(L)/minor(L) and minor(L′)/major(L′). It is clear that the ν(CO) spectral lineshape of the intervalence charge transfer (−1) state of **1** (Figure 3 and 4) is too extensively overlapped to be interpreted meaningfully within the context of Figure 4. However, a remarkable simplification of the spectrum can be realized by selectively labeling one Ru_3 cluster with $^{13}C^{18}O$ while the other contains a CO ligand with natural abundances of isotopes (mostly $^{12}C^{16}O$). Such an isotopic substitution has the effect of shifting the $\nu(^{13}C^{18}O)$ frequencies some 85 cm^{-1} lower in energy than the $\nu(^{12}C^{16}O)$ bands. This has the additional effect of separating in frequency the major(L)/minor(L) exchange pair spectral components by 85 cm^{-1} from the minor(L′)/major(L′) pair in the mixed valence (−1) state. Figure 5 shows the ν(CO) spectra of $[Ru_3O(OAc)_6(L)(CO)(\mu\text{-pz})Ru_3O(OAc)_6(L')(^{13}C^{18}O)]$ (L = dmap, L′ = py (**1***); L = py, L′ = cpy (**2***); L = dmap, L′ = cpy (**3***)) in the neutral (0), mixed valence (−1), and doubly reduced (−2) states. The spectra of the neutral and −2 states each show two single ν(CO) bands, in which the lower-frequency band in each case corresponds to the $^{13}C^{18}O$ labeled Ru_3 cluster. The mixed valence (−1) states show two broad ν(CO) bands, each with a distinct shoulder on the inside. The overall spectra of the mixed valence (−1) states, Figure 5 (middle row), are precisely the results predicted for separating the nested major(L)/minor(L) and minor(L′)/major(L′) pairs of spectral

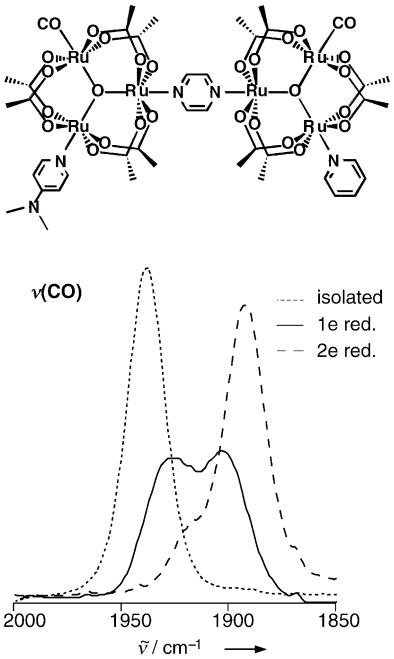

Figure 3. IRSE responses of **1** in the neutral (0) (....), mixed valence (−1) (——), and doubly reduced (−2) (-----) states. IRSE data were obtained at 233 K by using a low temperature thin layer cell[6] in CH_2Cl_2 solutions that contained 0.1 M tetrabutylammonium hexafluorophosphate as the supporting electrolyte.

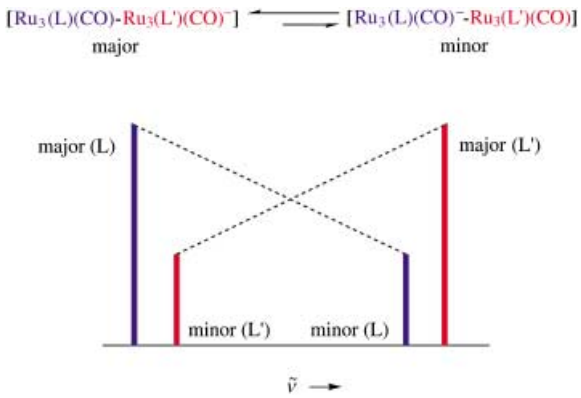

Figure 4. Schematic of exchange pairs in ν(CO) IR spectra of $\mathbf{1}^-$–$\mathbf{3}^-$. In the case where major and minor charge-transfer isomers exist, four peaks are expected. The resulting lineshapes are determined by both the relative populations (equilibrium constant) of major and minor isomers and the electron transfer rate constants that will tend to coalesce the spectral components that correspond to major(L)/minor(L) and minor(L′)/major(L′).

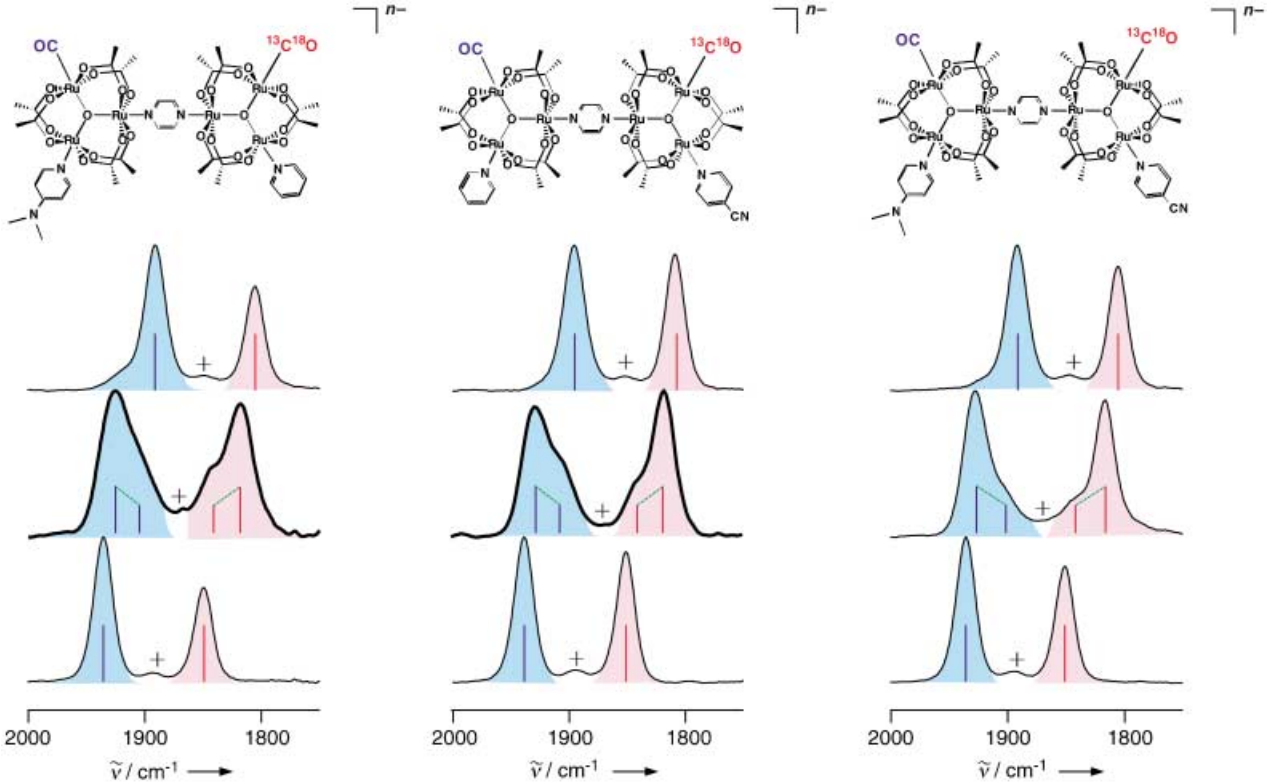

Figure 5. IRSE data for **1***, **2***, **3*** in the neutral (0; bottom row of spectra), mixed valence (−1; middle row of spectra), and doubly reduced (−2; top row of spectra) states. The small peaks identified by the "+" symbol correspond to $^{13}C^{16}O$ isotopic impurities.

components depicted in Figure 4 by isotope shifts. The peak assignments for the ν(CO) spectra of **1***, **2***, and **3*** in Figure 5 then in each case are (from high frequency to low frequency): major(L), minor(L), minor(L′), major(L′). These spectra provide compelling evidence for the presence of two charge transfer isomers. The fact that the bands are overlapped and broadened provides additional evidence that electron transfer is occurring to interconvert the charge transfer isomers on the IR timescale.

The IR spectra of **1***, **2***, and **3*** were analyzed by dynamic IR simulation with a modified version of VIBEXGL,[3,7] to obtain both the thermodynamics (major/minor equilibrium constant, K_{eq}, and derived free energy difference, ΔG_1) and kinetics (k_+, the rate constant for "uphill" (major→minor) ET) for charge-transfer isomers (see Table 1. It is clear that the populations of the minor isomers are far in excess of predictions based on differences in intrinsic reduction potentials. The values of K_{eq} predicted from ΔG_0 range from 150 (**1**) to 91 000 (**3**) (Table 1). The experimentally determined values of K_{eq} range from 1.6 (**1**) to 3.4 (**3**). The reason that charge transfer isomers can be observed in the present study then must be that the mixed valence (−1) states of **1**–**3** are so strongly electronically coupled that the diabatic free energies, ΔG_0, of 810–1850 cm^{-1} are reduced to (adiabatic) ΔG_1 values of only 75–200 cm^{-1}. The ν(CO) spectra in the mixed valence (−1) state (Figure 5) for each of **1***, **2***, and **3*** showed very small temperature dependence in favor of the major isomer at lower temperature in the range available experimentally (−40 to 7 °C). However, the spectral changes were so small

Table 1: Data for complexes **1**, **2**, and **3**.[a]

L-L′	ΔG_0 [cm^{-1}]	predicted (233 K)	actual (233 K)	ΔG_1 [cm^{-1}]	k_+ [$\times 10^{11}$ s^{-1}]
dmap-py (**1**)	810	150	1.6 ± 0.1	75	8.5 ± 0.5
py-cpy (**2**)	1050	650	2.4 ± 0.2	140	3.0 ± 0.5
dmap-cpy (**3**)	1850	91 000	3.4 ± 0.2	200	0.4 ± 0.2

[a] Diabatic and adiabatic free energies and equilibrium constants, experimentally determined total reorganization energies, and experimentally determined rate constants for forward electron transfer in the asymmetric charge transfer states.

(comparable to experimental error) that the effect of temperature on k_+ and K_{eq} could not be determined quantitatively.

Perhaps the most surprising result of the present study is that the large magnitudes of H_{AB} that evidently are sufficient to nearly equalize the populations of major and minor charge-transfer isomers are not sufficient to fully delocalize the systems to states with a single minimum. For example, Figure 6 presents the computed results of potential-energy surfaces developed by Sutin,[8] assuming an initial diabatic $\Delta G_0 = 810\ cm^{-1}$ and total reorganization energy $\lambda = 11\,500\ cm^{-1}$ ($\tilde{\nu}_{max}$ in ref. [6]), similar to values determined for **1**, as a function of increased electronic coupling, H_{AB}. At the point that the adiabatic free energy difference is diminished to $\Delta G_1 = 520\ cm^{-1}$ (for $H_{AB} = 4260\ cm^{-1}$), the double minimum required for two charge-transfer isomers is

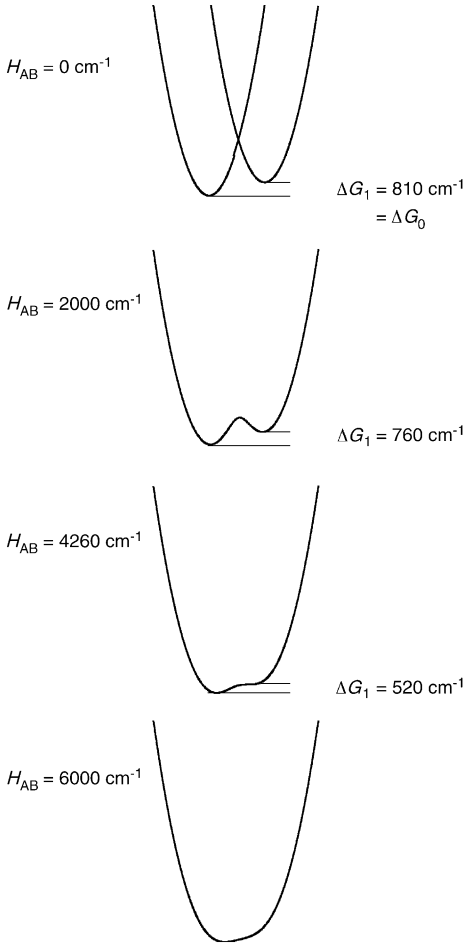

Figure 6. Diabatic (top) and adiabatic potential-energy surfaces showing how the Gibbs free-energy difference for electron transfer, ΔG_1, decreases as the electronic coupling, H_{AB}, increases. The potentials used[8] suggest that a single minimum (fully delocalized system) is attained at a value of $H_{AB} = 4260\ cm^{-1}$ if the initial diabatic driving force, ΔG_0, is 810 cm^{-1}.

no longer defined. Experimentally, we observe clear evidence of a double minimum: the presence of two charge-transfer isomers with relative populations 1.6:1, corresponding to $\Delta G_1 = 75\ cm^{-1}$. Why then, do these unusual complexes continue to exhibit dynamic exchange between alternate structures when they might otherwise achieve a single delocalized structure? It appears likely that these systems remain coupled to some other local dynamics (e.g., solvent, or molecular normal modes)[9,10] such that the equilibrated structure required for full electronic delocalization cannot be achieved. Experimental evidence of solvent control of the rates of ET in symmetrical systems related to **1–3** was reported recently.[11] Further studies should clarify the relative importance of local solvent and internal normal mode dynamics to the existence of charge transfer isomers.

Experimental Section

Preparation of **1–3**: The asymmetric dimers **1–3** were prepared in a way similar to the symmetric dimers by reacting equimolar quantities of $[Ru_3(\mu_3\text{-}O)(\mu\text{-}CH_3CO_2)_6(CO)(L)(H_2O)]$ and $[Ru_3(\mu_3\text{-}O)(\mu\text{-}CH_3CO_2)_6(CO)(L')(pz)]$. The dmap–py dimer,**1**, was prepared as follows. A mixture of $[Ru_3(\mu_3\text{-}O)(\mu\text{-}CH_3CO_2)_6(CO)(py)(H_2O)]$ (62 mg, 0.0775 mmol) and $[Ru_3(\mu_3\text{-}O)(\mu\text{-}CH_3CO_2)_6(CO)(dmap)(pz)]$ (70 mg, 0.0775 mmol) in CH_2Cl_2 (15 mL) was allowed to stand for 2 days at room temperature. The resulting solution was subjected to chromatography over silica gel with CH_2Cl_2/MeOH 99:1 (volume/volume) as the eluting agent. The compound was isolated from the main blue-green band. Yield 103 mg, 74%. Compounds **2** and **3** were prepared in a similar way with the use of appropriate Ru_3 cluster. For **1:** Elemental analysis (%) calcd for $Ru_6C_{42}H_{55}O_{28}N_5$: C 29.95, H 3.29, N 4.16; found: C 29.22, H 3.44, N 4.18. FABMS: *m*/*z* 1659, 1629 (calcd $[M-CO] = 1656$, $[M-2CO] = 1628$). ^{1}H NMR (270 MHz, $CDCl_3$): $\delta = 9.31$ (2H, pz), 9.21 (2H, py-*o*), 8.94 (2H + 2H, dmap-*o*, pz), 8.16 (1H, py-*p*), 8.07 (2H, py-*m*), 7.25 (2H, dmap-*m*), 3.34 (6H, dmap CH_3), 2.25 (6H, acetate CH_3), 2.21 (6H, acetate CH_3), 2.16 (6H, acetate CH_3), 2.11 (6H, acetate CH_3), 2.00 (6H, acetate CH_3), 1.95 ppm (6H, acetate CH_3). For **2:** Elemental analysis (%) calcd for $Ru_6C_{41}H_{49}O_{28}N_5{\cdot}3H_2O$: C 28.62, H 3.22, N 4.07%; found: C 28.47, H 3.11, N 4.10%. FABMS: *m*/*z* 1666, 1638, 1611 (calcd $[M] = 1667$, $[M-(CO)] = 1638$, $[M-2CO] = 1611$). ^{1}H NMR (270 MHz, $CDCl_3$): $\delta = 9.22$ (2H, pz), 9.09 (2H, py-*o*), 8.93 (2H, pz), 8.21 (2H, cpy-*m*), 8.15 (1H, py-*p*), 8.06 (2H, py-*m*), 2.26 (6H, acetate CH_3), 2.24 (6H, acetate CH_3), 2.18 (6H, acetate CH_3), 2.16 (6H, acetate CH_3), 2.03 (6H, acetate CH_3), 1.99 ppm (6H, acetate CH_3). For **3:** Elemental analysis (%) calcd for $Ru_6C_{43}H_{54}O_{28}N_5{\cdot}5H_2O$: C, 28.70, H, 3.59, N, 4.67%. Found: C 28.80, H 3.57, N 4.73%. FABMS: *m*/*z* 1653 (calcd $[M-2CO] = 1653$). ^{1}H NMR (270 MHz, $CDCl_3$): $\delta = 9.30$ (2H, pz), 9.08 (2H, pz), 8.92 (2H, dmap-*o*), 8.79 (2H, cpy-*o*), 8.22 (2H, cpy-*m*), 7.23 (2H, dmap-*m*), 3.34 (6H dmap CH_3), 2.26 (6H, acetate CH_3), 2.20 (6H, acetate CH_3), 2.18 (6H, acetate CH_3), 2.11 (6H, acetate CH_3), 2.03 (6H, acetate CH_3), 1.95 ppm (6H, acetate CH_3).

Preparation of **1***–**3***: Asymmetric dimers with $^{13}C^{18}O$ ligand were prepared similarly to the above mentioned method for **1–3** by using corresponding Ru_3 cluster with $^{13}C^{18}O$ ligand. $[Ru_3(\mu_3\text{-}O)(\mu\text{-}CH_3CO_2)_6(^{13}C^{18}O)(H_2O)(L)]$ was synthesized from $[Ru_3(\mu_3\text{-}O)(\mu\text{-}CH_3CO_2)_6(^{13}C^{18}O)(H_2O)_2]$. In all cases, isotopically labeled $^{13}C^{18}O$ was introduced onto the Ru_3 cluster fragment having the lower reduction potential. This produces the least complicated spectral overlaps of the ν(CO) spectra in the −1 states.

Received: November 3, 2003 [Z53221]

Keywords: charge transfer · electrochemistry · electron transfer · IR spectroscopy · mixed-valent compounds

[1] T. Ito, T. Hamaguchi, H. Nagino, T. Yamaguchi, H. Kido, I. S. Zavarine, T. Richmond, J. Washington, C. P. Kubiak, *J. Am. Chem. Soc.* **1999**, *121*, 4625–4632.

[2] T. Ito, T. Hamaguchi, H. Nagino, T. Yamaguchi, J. Washington, C. P. Kubiak, *Science* **1997**, *277*, 660–663.

[3] F.-W. Grevels, K. Kerpen, W. E. Klotzbücher, R. E. D. McClung, G. Russell, M. Viotte, K. Schaffner, *J. Am. Chem. Soc.* **1998**, *120*, 10423–11043.

[4] The intrinsic reduction potentials are taken as the mean value of (0/−1) and (−1/−2) reduction potentials in the symmetrically ligand substituted (dmap–dmap, py–py, and cpy–cpy) dimers.[1] In this case, the potentials for the (0/−1) and (−1/−2) redox couples are split only by electronic interactions. The mean value reflects the intrinsic reduction potential for one Ru3 cluster with a given ligand substitution in a dimer together with another similarly substituted Ru_3 cluster.

[5] Intervalence-transfer (IT) electronic-absorption spectroscopic data for the mixed valence (−1) states of **1–3**. $\tilde{\nu}_{max}$ (ε_{max}) = 11500 (16600) for **1**, 10500 (12200) for **2** and 10400 cm^{-1} (10100 $M^{-1}cm^{-1}$) for **3**.

[6] I. S. Zavarine, C. P. Kubiak, *J. Electroanal. Chem.* **2001**, *495*, 106 – 109.
[7] R. E. D. McClung in *VibexGL: Program for the Simulation of IR Spectra of Exchanging Systems.*
[8] N. S. Sutin, *Prog. Inorg. Chem.* **1983**, *30*, 441 – 498.
[9] D. V. Matyushov, G. A. Voth, *J. Phys. Chem. A* **2000**, *104*, 6470 – 6484.
[10] K. D. Demadis, C. M. Hartshorn, T. J. Meyer, *Chem. Rev.* **2001**, *101*, 2655 – 2685.
[11] C. H. Londergan, J. C. Salsman, S. Ronco, L. M. Dolkas, C. P. Kubiak, *J. Am. Chem. Soc.* **2002**, *124*, 6236 – 6237.

